Tuning band gaps in twisted bilayer MoS₂

Yipei Zhang,[1] Zhen Zhan ●,[1,*] Francisco Guinea,[2,3] Jose Ángel Silva-Guillén ●,[1] and Shengjun Yuan ●[1,†]

[1]*Key Laboratory of Artificial Micro- and Nano-structures of Ministry of Education and School of Physics and Technology, Wuhan University, Wuhan 430072, China*
[2]*Fundación IMDEA Nanociencia, C/Faraday 9, Campus Cantoblanco, 28049 Madrid, Spain*
[3]*Donostia International Physics Center, UPV/EHU, 20018 San Sebastián, Spain*

In the emerging world of twisted bilayer structures, the possible configurations are limitless, which enables a rich landscape of electronic properties. In this paper, we focus on twisted bilayer transition metal dichalcogenides (TMDCs) and study their properties by means of an accurate tight-binding model. We build structures with different angles and find that the so-called flat bands emerge when the twist angle is sufficiently tiny (smaller than 7.3°). Interestingly, the band gap can be tuned up to 5% (107 meV) when the twist angle in the relaxed sample varies from 21.8° to 0°. Furthermore, when looking at the local density of states we find that the band gap varies locally along the moiré pattern due to the change in the coupling between layers at different sites. Finally, we also find that the system can suffer a transition from a semiconductor to a metal when a sufficiently strong electric field is applied. Our study can serve as a guide for the practical engineering of TMDC-based optoelectronic devices.

I. INTRODUCTION

Although graphene has been known for some time now [1], recently, there has been renewed interest in the properties of bilayer structures due to the discovery of strongly correlated effects in these structures at certain small (magic) twist angles [2]. This finding triggered a handful of experimental and theoretical studies into that kinds of structures in which not only strongly correlated effects such as superconductivity and quantum phase transitions [3–13] but also the existence of pseudomagnetic fields due to the strain that the system can experience by externally applying a mechanical strain [14,15] or due to intrinsic strain that appears in the moiré pattern because of the incommensurability of the superstructures [16] can occur.

Similar to graphene, group V-B transition metal dichalcogenides (TMDCs) are exfoliated materials that have a hexagonal structure and also change their electronic properties dramatically when lowering the number of layers to one. Interestingly, in contrast to graphene, TMDCs are semiconductors, and moreover, the nature of the band gap depends on the number of layers changing from indirect to direct when the system goes from multilayer to monolayer [17]. The fact that monolayer TMDCs present a direct band gap overcomes one of the major drawbacks of graphene for its integration in modern electronic and optoelectronic devices. Furthermore, this band gap can be tuned by means of the so-called strain-tronics [18] methods or electric fields. Therefore, it seems like a natural and interesting step to study the electronic proper-

ties of twisted bilayer TMDCs. Recently, a theoretical work using density functional theory (DFT) methods predicted the existence of flat bands in MoS₂ when the twist angle is sufficiently small [19]. Furthermore, an experimental work was carried out on another twisted bilayer TMDCs, WSe₂, that found such flat bands when achieving small twist angles [20]. Interestingly, it has been shown that the different environment surrounding the atoms due to the change in the stacking along the moiré pattern in heterobilayer TMDCs (a structure formed by a different TMDCs in each layer) entails a difference in the interlayer coupling, which results in a local change in the gap [21]. Nevertheless, a thorough study of the electronic properties and their possible tunability of the twisted bilayer TMDCs is still lacking.

In this work, we study the electronic properties of twisted bilayer MoS₂ and the possibility of tuning the band gap. This paper is organized in the following way: We first show how to build the commensurate twisted bilayer TMDCs and the method used to compute their electronic properties. Then, we study the tunability of these properties by means of a change in the rotation angle by the variation of the local interlayer couplings due to the different stackings in the moiré pattern or by applying an electric field to the system.

II. THE COMMENSURATE BILAYERS

We consider bilayer TMDCs, which are composed of two monolayers of MoS₂ rotated in the plane by an angle θ. Since the two layers have the same lattice constant, following the same method as in twisted bilayer graphene, the moiré super-cell can be constructed by identifying a common periodicity between the two layers [5]. We start with the 2H stacking ($\theta = 0°$) of MoS₂, that is, with the Mo (S) atom in the top

---

*zhen.zhan@whu.edu.cn
†s.yuan@whu.edu.cn
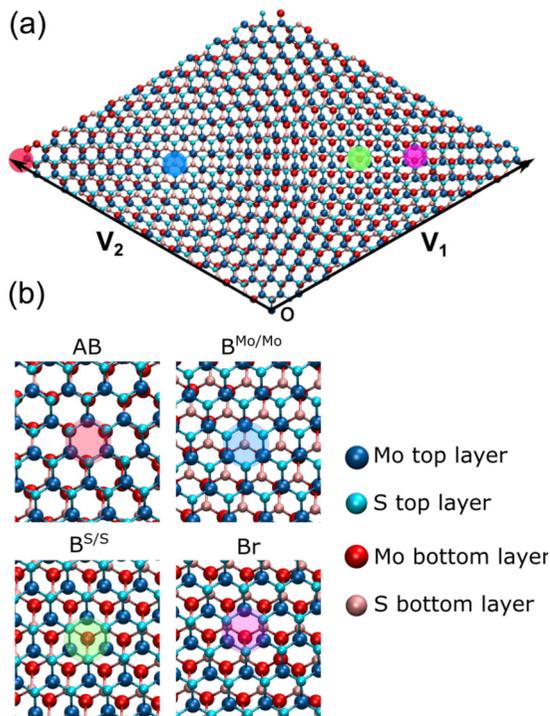
FIG. 1. (a) The moiré superlattice of twisted bilayer MoS$_2$ with rotation angle $\theta = 3.5°$. (b) Zoom around the atomic structures of different high-symmetry points. The AB, B$^{Mo/Mo}$, B$^{S/S}$, and Br regions are highlighted by circles of different colors.

layer directly above the S (Mo) in the bottom layer, and choose the rotation origin (O) at an atom site. For the top layer, we define a supercell with a basis vector $\mathbf{V_1}(n, m) = n\mathbf{a_1} + m\mathbf{a_2}$, where $\mathbf{a_1}$ and $\mathbf{a_2}$ are the lattice vectors of single-layer MoS$_2$ and n and m are non-negative integers with $n - m = 1$, which means that the supercell contains only one moiré pattern. For the bottom layer, a cell with the same size and rotated by an angle θ can be obtained with the basis vector $\mathbf{V_1'}(m, n)$. Then, the commensurate bilayers with the twist angle θ can be achieved by rotating the top cell with $\mathbf{V_1}$ by $\theta/2$ and rotating the bottom cell with $\mathbf{V_1'}$ by $-\theta/2$. The rotation angle is given by

$$\cos\theta = \frac{n^2 + 4nm + m^2}{2(n^2 + nm + m^2)}. \tag{1}$$

The commensurate supercell contains $N = 6(n^2 + nm + m^2)$ atoms, and the lattice vectors are $\mathbf{V_1}$ and $\mathbf{V_2} = -m\mathbf{a_1} + (n + m)\mathbf{a_2}$, with $|\mathbf{V_1}| = |\mathbf{V_2}| = \frac{a}{2\sin(\theta/2)}$, where $a = 3.16$ Å is the lattice constant of the single-layer MoS$_2$ [22]. Figure 1(a) shows a twisted bilayer MoS$_2$ structure with a twist angle $\theta = 3.5°$, which is obtained with $n = 10$ and $m = 9$. The moiré superlattice contains 1626 atoms. In a supercell with a relatively small twist angle there are several high-symmetry stacking patterns, for instance, AB, B$^{Mo/Mo}$, and B$^{S/S}$. In the AB stacking, the Mo atoms of layer 1 are over the S atoms of layer 2, and the S atoms of layer 1 are over the Mo atoms of layer 2. For B$^{Mo/Mo}$, Mo atoms of layer 1 are over Mo atoms of layer 2, and all S atoms of one layer are located in the center of hexagons of the other layer. For B$^{S/S}$, S atoms of layer 1 are over S atoms of layer 2, and all Mo atoms of one layer are in

the center of hexagons of the other layer. The Br site is located at one third of the B$^{S/S}$–AB path. All of these special sites are illustrated in Fig. 1(b).

III. NUMERICAL METHOD

Ultraflat bands at the valence band edge were discovered theoretically in twisted bilayer MoS$_2$ [19,23,24]. Up to now, the largest system of this kind of calculation using first-principles methods contained 4902 atoms, which corresponds to a twist angle of $2.0°$. Although it is possible to perform calculations on larger systems, there are some limitations due to the computational resources when the twist angle becomes smaller since the number of atoms increases sharply. A systematic study of these larger systems can be more easily done by utilizing a tight-binding method. For instance, the system with the electronic properties calculated by diagonalization in reciprocal space contains up to 59 644 orbitals, which corresponds to $\theta = 1°$.

In this paper, we will use another approach, the tight-binding propagation method (TBPM), to investigate the electronic properties of twisted bilayer MoS$_2$. The TBPM is based on the numerical solution of the time-dependent Schrödinger equation without any diagonalization [25]. Both memory and CPU costs scale linearly with the system size. Therefore, the TBPM can tackle systems with the number of orbitals being as large as 10 million, for instance, extremely tiny twist angles in twisted bilayer graphene [16] and bilayer graphene quasicrystals [26]. More importantly, defects and magnetic and electric fields can be easily implemented in this approach. We briefly outline the main formalism of using the TBPM to calculate the density of the states (DOS). TBPM starts with a random superposition of basis function $|\phi_0\rangle = \sum c_i |a_i\rangle$, where c_i are random complex numbers and $|a_i\rangle$ are basis states of the calculated sample. Then, by solving the time-dependent Schrödinger equation, the DOS is obtained from the Fourier transform of the time-dependent correlation function: $d(\epsilon) = \frac{1}{2\pi} \int_{-\infty}^{+\infty} e^{i\epsilon\tau} \langle\phi_0|e^{-iH\tau/\hbar}|\phi_0\rangle d\tau$, where H is the Hamiltonian of the system. In this method, the accuracy is determined by the number of orbitals in the sample and can be increased by using larger samples or averaging results from different random initial states. The number of time integration steps determines the energy resolution. The larger the system is, the more accurate the calculated results are. Such a method was implemented in our home-made program TIPSI (tight-binding propagation simulator), where the density of the states, local density of states, quasieigenstates, and many other electronic and optical properties can be easily obtained once the Hamiltonian of the system is given.

In order to calculate the electronic band structures of twisted bilayer TMDCs, we use the accurate tight-binding Hamiltonian introduced in Ref. [27]. The minimum atomic orbital bases to correctly describe monolayer TMDCs are the five d orbitals of the transition-metal atom and three p orbitals of each of the two chalcogen atoms [28,29]. This model well reproduces the band structure calculated using DFT with GW quasiparticle correction in the low-energy region. For bilayer TMDCs, the total Hamiltonian can be written as [27,30]

$$\hat{H} = \hat{H}_1^{(1L)} + \hat{H}_2^{(1L)} + \hat{H}_{int}^{(2L)}, \tag{2}$$

where $\hat{H}_{1(2)}^{(1L)}$ is the 11-orbital single-layer Hamiltonian and $\hat{H}_{1(2)}^{(2L)}$ is the interlayer Hamiltonian. $\hat{H}_{1(2)}^{(1L)}$ contains the on-site energy, the hopping terms between orbitals of the same type at first-neighbor positions, and the hopping terms between orbitals of different types at first- and second-neighbor positions. The interlayer hopping Hamiltonian includes only the interaction between the chalcogen atoms at the interface of the bilayer:

$$\hat{H}_{int}^{2L} = \sum_{p_i',\mathbf{r}_2,p_j,\mathbf{r}_1} \hat{\phi}_{2,p_i'}^{\dagger}(\mathbf{r}_2) t_{p_i',p_j}^{(LL)}(\mathbf{r}_2 - \mathbf{r}_1) \hat{\phi}_{1,p_j}(\mathbf{r}_1)$$
$$+ \text{H.c.}, \tag{3}$$

where $\hat{\phi}_{i,p_j}$ is the p_j orbital basis of the ith monolayer. Within the Slater-Koster approximation, the hopping terms can be expressed as

$$t_{p_i',p_j}^{(LL)}(\mathbf{r}) = [V_{pp,\sigma}(r) - V_{pp,\pi}(r)]\frac{r_i r_j}{r^2} + V_{pp,\pi}(r)\delta_{i,j}, \tag{4}$$

where $r = |\mathbf{r}|$ and the distance-dependent Slater-Koster parameter is

$$V_{pp,b} = v_b e^{[-(r/R_b)^{\eta_b}]}, \tag{5}$$

where $b = \sigma, \pi, v_b, R_b$, and η_b are constant values that depend on the specific chalcogen interlayer interactions, for which values are taken from Ref. [27]. In our calculations, we include only the interlayer hopping terms between a pair of chalcogen atoms that are separated by a distance smaller than 8 Å.

In all the calculations, we use a large enough system with more than 10 million orbitals to ensure the convergence of the results. For instance, the number of orbitals in the unit cell of twisted bilayer MoS₂ with $\theta = 2.0°$ is 17 974. To perform the calculation with the TBPM, we use a large sample containing 31×31 unit cells. The time steps are set to 4096, which gives an energy resolution of 1.8 meV. Periodic boundary conditions are used in the simulation. Furthermore, we can use TBPM to obtain the map of the amplitudes of the quasieigenstates, which has been shown to be in agreement with the measured dI/dV mapping in experiments (for instance, the results in Ref. [16]). Note that the band structure calculations in Sec. IV C are performed by standard diagonalization of the Hamiltonian in Eq. (2).

IV. Results and Discussion

A. Tuning the band gap by rotation angle

It has been proven that the twist angle has significant influence on the electronic properties of twisted bilayer TMDCs [31–35]. All these studies were mainly focused on large rotation angles. Interestingly, ultraflat bands have been detected in low-angle twisted bilayer MoS₂. These flat bands provide a good platform to explore new physical phenomena, for instance, the Mott-insulating phase at half filling of the band [2,19]. This leaves important questions unaddressed: Are there ultraflat bands in twisted TMDCs with a tiny twist angle? What exotic features will be found in low-angle twisted bilayer TMDCs?

In this part, we study the density of states of twisted bilayer MoS₂ with various rotation angles. The smallest rotation angle that we calculate is 0.8°, which results in a moiré pattern that contains 29 526 atoms (108 262 orbitals). It is far beyond the ability of state-of-the-art first-principles methods and tight-binding methods where the electronic structure is calculated by using diagonalization methods. The DOS of rigidly twisted bilayer MoS₂ with angles changing from 0° to 21.8° is plotted in Fig. 2(a). It is clear that the DOS varies significantly depending on the angle, especially for the DOS deep in the valence band, which is in good agreement with the calculated results in Ref. [36]. More interesting things happen near the band edges. In order to investigate this, the detailed evolution of DOS near the band edge is illustrated in Figs. 2(b) and 2(c). We see clearly that, except for the 0° angle that corresponds to the 2H stacking, as the twist angle decreases, the conduction band edge energy decreases, and the energy gap decreases. That is, the band gap can be engineered through the control of the rotation angle. As shown in Fig. 3 (black line), the band gap reduces by 104 meV (around 5% change) when changing the rotation angle from 21.8° to 0.8°. Note that, for samples with small twist angles, some energy peaks appearing near the valence band edges correspond to the detected ultraflat bands. For instance, in the DOS of the twisted bilayer MoS₂ with twist angle $\theta = 3.5°$, the peak located at −0.2 eV corresponds to the ultraflat band discovered in Refs. [19,37]. In principle, for rigidly twisted MoS₂ with rotation angles below a crossover value $\theta^* \approx 7°$, the isolated flat band emerges, and the states of the flat band in the valence band maximum (VBM) are localized in the $B^{S/S}$ region
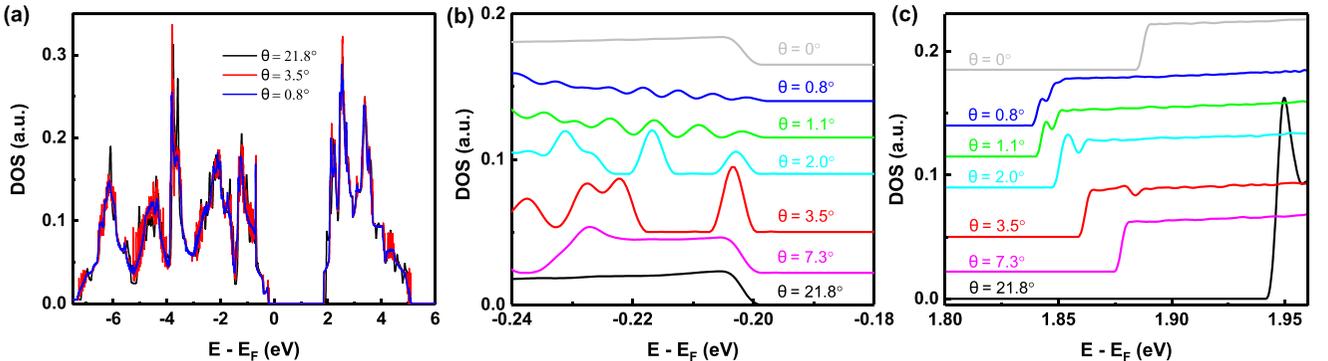
FIG. 2. (a) The calculated DOS of rigidly twisted bilayer MoS₂ with different twist angles. (b) and (c) The detailed changes in the DOS near the valence and conduction band extrema, respectively.
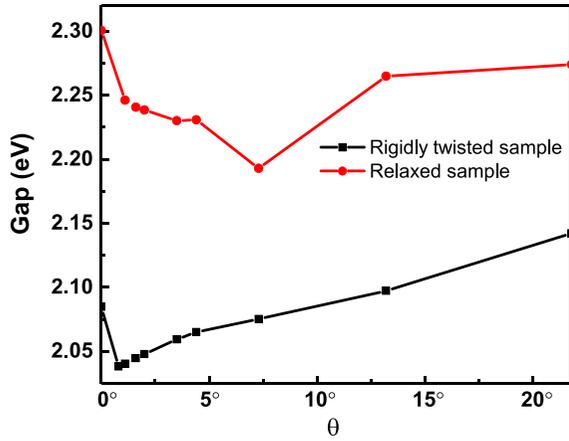
FIG. 3. The band gap E_g between the CBM and VBM of twisted bilayer MoS_2 with different rotation angles. The black and red lines are for unrelaxed and relaxed cases, respectively.

(see Sec. IV B). This result is consistent with reported experimental and DFT results [19,20].

Next, we investigate the influence of the lattice relaxation on the band gap of twisted bilayer MoS_2 with various rotation angles. The structural relaxations are performed with the LAMMPS [38,39] package, in which the Stillinger-Weber potential [40] for interactions between atoms within the layer and the Lennard-Jones potential [41] for interlayer interactions are implemented. The minimizations are performed using the conjugate gradient method with the energy tolerance being 10^{-15} eV. The relaxed sample is assumed to keep the period of the rigidly twisted MoS_2. The lattice relaxation leads to the variation of the interatomic bond lengths, which modifies both the interlayer and intralayer hoppings in Eq. (2). The interlayer hopping changes according to Eq. (5), and the distance-dependent intralayer hopping can be written as [42]

$$t_{ij,\mu\nu}^{\text{intra}}(\mathbf{r}_{ij}) = t_{ij,\mu\nu}^{\text{intra}}(\mathbf{r}_{ij}^0)\left(1 - \Lambda_{ij,\mu\nu}\frac{|\mathbf{r}_{ij} - \mathbf{r}_{ij}^0|}{|\mathbf{r}_{ij}^0|}\right), \quad (6)$$

where $t_{ij,\mu\nu}^{\text{intra}}$ is the intralayer hopping between the μ orbital of the ith atom and ν orbital of the jth atom, $\mathbf{r}_{ij}^0$ and $\mathbf{r}_{ij}$ are the distance between the ith and jth atoms in the equilibrium and relaxed cases, and $\Lambda_{ij,\mu\nu}$ is the dimensionless bond-resolved local electron-phonon coupling. We assume that $\Lambda_{ij,\mu\nu} = 3, 4, 5$ for the S-S pp, S-Mo pd, and Mo-Mo dd hybridizations, respectively [42]. As we can see from the red line in Fig. 3, the minimum band gap appears at the twisted MoS_2 with $\theta = 7.3°$. The band gap declines 108 meV from $\theta = 0°$ to $7.3°$. Moreover, the lattice relaxation increases the band gap for all the twisted samples. In the tiny twist angle, the reduction of the band gap is compensated by the lattice relaxation. As we know, the relaxation effect is more significant in samples with a small rotation angle. So we can see from the red line in Fig. 3 that the band gap changes more smoothly in the tiny twist angles. Such a relaxation effect can be suppressed when placing the sample on a hexagonal BN substrate [43,44].
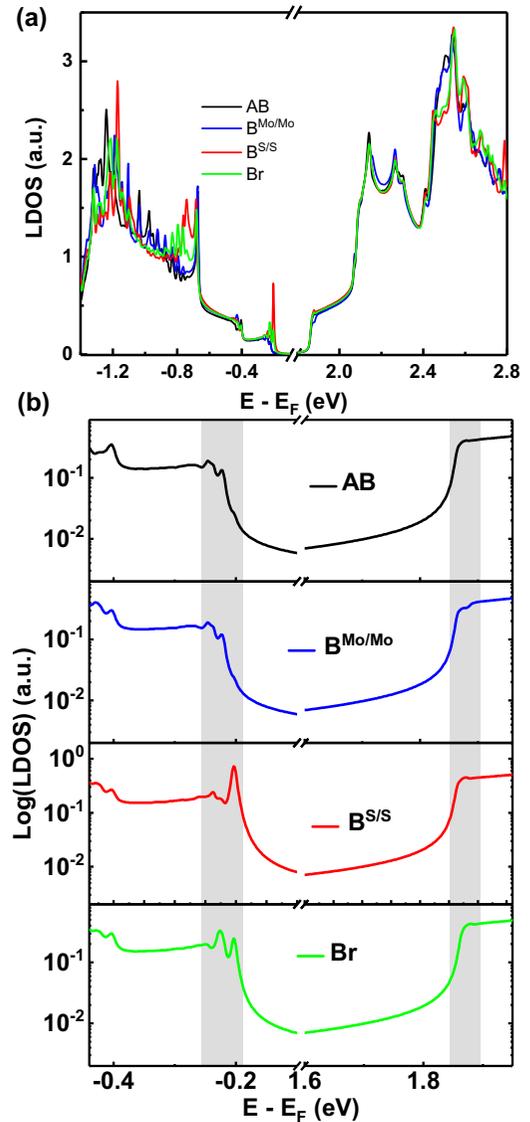
FIG. 4. (a) The calculated LDOS in the AB, $B^{Mo/Mo}$, $B^{S/S}$, and Br regions in a rigidly twisted bilayer MoS_2 sample with $\theta = 3.5°$. (b) The logarithmic scales of the LDOS near the valence and conduction band edges.

B. Tuning the band gap by interlayer coupling at different high-symmetry stacking points

It has been shown experimentally that, for heterostructures composed of monolayers of two different TMDCs, the local band gap is periodically modulated by the interlayer coupling at different high-symmetry points with an amplitude of ~ 0.15 eV [21]. Can the interlayer coupling be used as a parameter to tune the local band gap for the twisted homobilayer TMDCs (the heterostructure composed of the same monolayer TMDCs)? To answer this question, we calculate the local density of states for the twisted bilayer MoS_2 with $\theta = 3.5°$ at the high-symmetry stacking points AB, $B^{Mo/Mo}$, $B^{S/S}$, and Br (illustrated in Fig. 1).

The results are shown in Fig. 4(a). Similar to the DOS in Fig. 2, the interlayer coupling changes also significantly the local DOS (LDOS) deep into the valence band. The details of the LDOS near the VBM and conduction band minimum
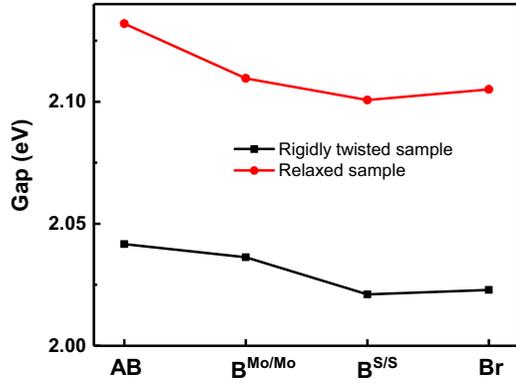
FIG. 5. The local band gap E_g of the AB, B$^{Mo/Mo}$, B$^{S/S}$, and Br regions in twisted bilayer MoS$_2$ with $\theta = 3.5°$. The black and red lines are for the rigid and relaxed cases, respectively.

(CBM) are plotted in Fig. 4(b). In the conduction band, the LDOSs near the band edge are similar for the four high-symmetry sites. On the contrary, the VBM has a remarkable change due to the different interlayer couplings at the four points, which can be seen more clearly in the logarithm of the LDOS illustrated in Fig. 4(b). Furthermore, we find in Fig. 4 that the ultraflat-band signature, which corresponds to a peak with energy ~ -0.2 eV, appears only at the B$^{S/S}$ and Br points. We can also see that the sharpest peak appears in B$^{S/S}$ sites. This is expected since at this position the top layer S atom sits directly above a bottom layer S atom, which gives the strongest interlayer interaction, given the fact that in our tight-binding model, interlayer coupling originates from hopping between S atoms in different layers. The absence of signals of the flat band in other areas indicates that the localization of the electronic states of the flat band is around the B$^{S/S}$ site, which is in accordance with the localization of the VBM wave function in the rigidly twisted sample in Ref. [19]. The local energy gap in different stacking regions is shown by the black line in Fig. 5. We can see how the band gap changes locally depending on the specific site. At B$^{S/S}$, which has the strongest interlayer coupling, we find the minimum local energy gap. The local band gap is modulated periodically with an amplitude of ~ 35 meV. The evolution of such a site-dependent local band gap is in agreement with the experimental results reported for heterostructure TMDCs [21]. In the relaxed case, as shown by the red line in Fig. 5, the minimum band gap is still located in the B$^{S/S}$ region, and the difference of the band gap at different high-symmetry points is ~ 31 meV. All in all, an important consequence of the interlayer coupling in the moiré supercell is the tuning the local band gap at different stacking points.

The periodic variation of the local electronic structure as a consequence of different interlayer couplings is also visualized more clearly by looking at the energy dependence of the spatial distribution of the LDOS plotted in Fig. 6. In the rigid cases, for instance, at a high negative energy of -2.06 eV, where a peak appears in the LDOS of the AA site, the spectrum at that same position is higher than that of the other three high-symmetry points. However, at an energy of around -0.2 eV, where the spectral feature of the AA site is out of the tunneling range, the intensity of the AA site
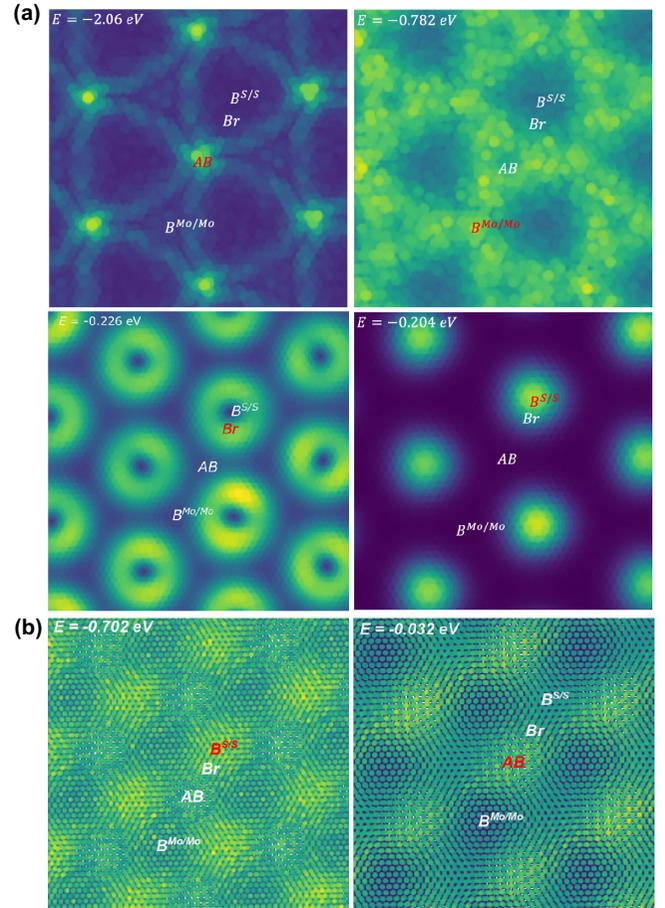
FIG. 6. Calculated LDOS mapping with different energies of the twisted bilayer MoS$_2$ with $\theta = 3.5°$ for the (a) rigid and (b) relaxed cases. The corresponding energies and the four special sites, AB, B$^{Mo/Mo}$, B$^{S/S}$ and Br, are labeled in each image.

changes from a bright feature to a deep hole, whereas the B$^{S/S}$ and Br sites have the highest spectral at energies -0.226 and -0.204 eV, respectively. As we discussed previously, all the states are localized around the B$^{S/S}$ site at -0.2 eV. The continuous evolution of the local electronic spectrum by different energies at different sites also occurs for positive energies (not shown here). For the relaxed sample, as shown in Fig. 6(b), the first flat band (-0.032 eV) in the VBM is mainly located at the AB site. The variation of the local electronic spectra at different sites also exists. However, the lattice relaxation weakens such variation. All in all, all these results show a periodic charge density modulation at different energies over large areas in both rigid and relaxed cases, which can be detected experimentally using scanning tunneling microscopy dI/dV mapping.

C. Tuning the band gap by applying an electric field

As has been shown, a vertical electric field can open a band gap in bilayer graphene [45,46]. Furthermore, bilayer TMDCs can suffer a transition from a semiconductor to a metal when the applied field is strong enough [47–49]. However, to date the effect of the electric field and the possible modulation of the band gap in small-angle twisted TMDCs has not been
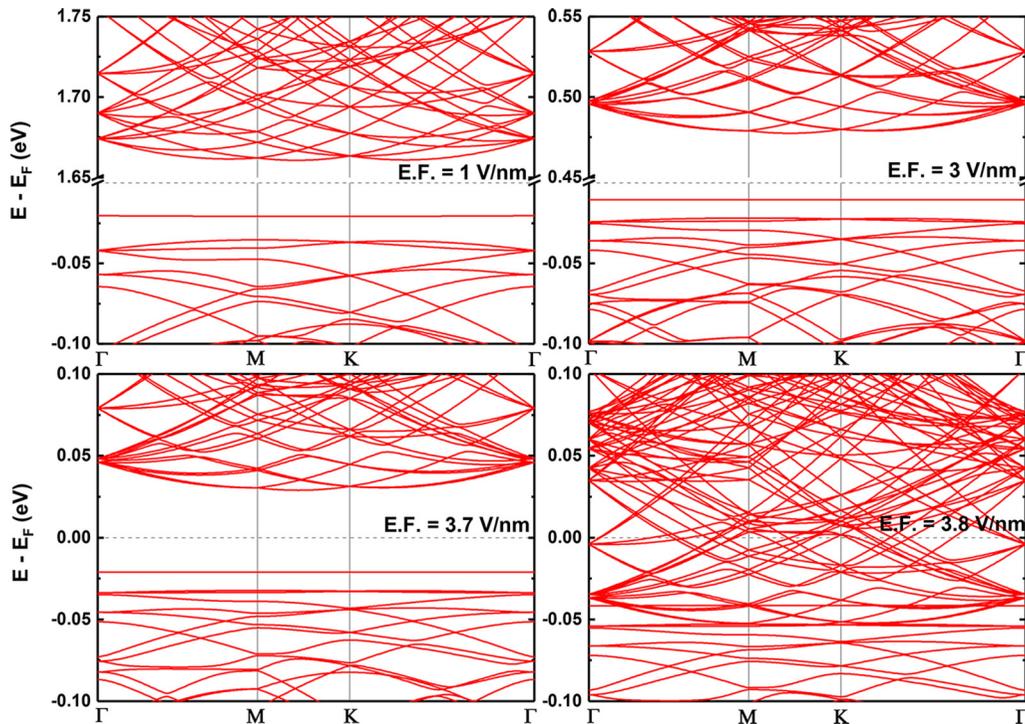
FIG. 7. Band structure of rigidly twisted bilayer MoS$_2$ with $\theta = 3.5°$ along the Γ-K-M-Γ direction in reciprocal space as a function of the applied external electric field. The band structures are obtained by exact diagonalization of the Hamiltonian in Eq. (2). Note that the vertical axis scales are different in each panel.

studied. Since all of these materials could be integrated into new electronic devices where a gate is applied, the study of this effect is of much interest. In this part, we investigate the band gap tuning in twisted bilayer TMDCs by an external electric field applied perpendicularly to the layers, in particular, the twisted bilayer MoS$_2$ with $\theta = 3.5°$.

Figure 7 shows the band structure of rigidly twisted bilayer MoS$_2$ with $\theta = 3.5°$ under four different strengths of external electric fields perpendicular to the layers. The band gap is driven linearly to zero as electric field E increases, and the system changes from a semiconductor to a metal when E is large enough. This can be easily understood thanks to the so-called giant Stark effect [50]. Due to the redistribution of the charge density on different layers when an electric field is applied, bands belonging to different layers are separated from each other, which results in the reduction of the energy gap. This same effect is also found in 2H stacking bilayer TMDCs [47,48] and large-angle twisted bilayer WS$_2$ [49]. The evolution of the band gap as a function of E for twisted bilayer MoS$_2$ with three different rotation angles is plotted in Fig. 8. Since the difference of the band gap in the three twist angles is quite small, the threshold values where the system becomes metallic do not change significantly with the twist angle. The band gaps in the relaxed samples are larger than that of the same rigid ones. Consequently, in the relaxed system, we would need a higher electric field to close the band gap.

V. CONCLUSION

In this paper we have studied the electronic properties of twisted bilayer MoS$_2$ and their possible tunability by means

of an accurate TBPM. We have seen that the flat band appears when reaching angles sufficiently small. Interestingly, we can tune the value of the gap up to 5% just by changing the rotation angle in relaxed systems. Furthermore, the gap is modulated at different high-symmetry positions of the structure due to the different interlayer couplings that appear. We have also shown that another effective method to tune the band gap is to apply a perpendicular electric field, In fact, the band gap diminishes with increasing electric field, and the
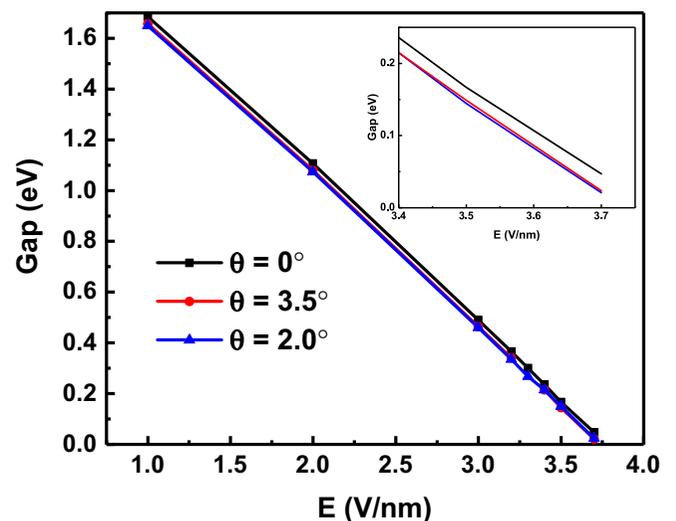
FIG. 8. The band gap of rigidly twisted bilayer MoS$_2$ with different rotation angles as a function of the applied external electric field.

system can undergo a transition from a semiconductor to a metal when the field is high enough.

ACKNOWLEDGMENTS

[1] K. S. Novoselov, A. K. Geim, S. V. Morozov, D. Jiang, Y. Zhang, S. V. Dubonos, I. V. Grigorieva, and A. A. Firsov, Science **306**, 666 (2004).

[2] Y. Cao *et al.*, Nature (London) **556**, 80 (2018).

[3] R. Bistritzer and A. H. MacDonald, Proc. Natl. Acad. Sci. USA **108**, 12233 (2011).

[4] G. Trambly de Laissardière, D. Mayou, and L. Magaud, Nano Lett. **10**, 804 (2010).

[5] G. Trambly de Laissardière, D. Mayou, and L. Magaud, Phys. Rev. B **86**, 125413 (2012).

[6] K. Kim, A. DaSilva, S. Huang, B. Fallahazad, S. Larentis, T. Taniguchi, K. Watanabe, B. J. LeRoy, A. H. MacDonald, and E. Tutuc, Proc. Natl. Acad. Sci. USA **114**, 3364 (2017).

[7] Y. Cao, V. Fatemi, S. Fang, K. Watanabe, T. Taniguchi, E. Kaxiras, and P. Jarillo-Herrero, Nature (London) **556**, 43 (2018).

[8] M. Yankowitz, S. Chen, H. Polshyn, Y. Zhang, K. Watanabe, T. Taniguchi, D. Graf, A. F. Young, and C. R. Dean, Science **363**, 1059 (2019).

[9] G. Chen *et al.*, Nat. Phys. **15**, 237 (2019).

[10] H. Yoo *et al.*, Nat. Mater. **18**, 448 (2019).

[11] A. Kerelsky *et al.*, Nature (London) **572**, 95 (2019).

[12] Y. Xie, B. Lian, B. Jäck, X. Liu, C.-L. Chiu, K. Watanabe, T. Taniguchi, B. A. Bernevig, and A. Yazdani, Nature (London) **572**, 101 (2019).

[13] Y. Jiang, X. Lai, K. Watanabe, T. Taniguchi, K. Haule, J. Mao, and E. Y. Andrei, Nature (London) **573**, 91 (2019).

[14] F. Guinea, M. Katsnelson, and A. Geim, Nat. Phys. **6**, 30 (2010).

[15] W. Yan, W.-Y. He, Z.-D. Chu, M. Liu, L. Meng, R.-F. Dou, Y. Zhang, Z. Liu, J.-C. Nie, and L. He, Nat. Commun. **4**, 2159 (2013).

[16] H. Shi *et al.*, Nat. Commun. **11**, 371 (2020).

[17] R. Roldán, L. Chirolli, E. Prada, J. A. Silva-Guillén, P. San-Jose, and F. Guinea, Chem. Soc. Rev. **46**, 4387 (2017).

[18] B. Amorim *et al.*, Phys. Rep. **617**, 1 (2016).

[19] M. H. Naik and M. Jain, Phys. Rev. Lett. **121**, 266401 (2018).

[20] Z. Zhang, Y. Wang, K. Watanabe, T. Taniguchi, K. Ueno, E. Tutuc, and B. J. LeRoy, Nat. Phys. **16**, 1093 (2020).

[21] C. Zhang, C.-P. Chuu, X. Ren, M.-Y. Li, L.-J. Li, C. Jin, M.-Y. Chou, and C.-K. Shih, Sci. Adv. **3**, e1601459 (2017).

[22] R. Roldán, J. A. Silva-Guillén, M. P. López-Sancho, F. Guinea, E. Cappelluti, and P. Ordejón, Ann. Phys. (Berlin, Ger.) **526**, 347 (2014).

[23] M. H. Naik, S. Kundu, I. Maity, and M. Jain, Phys. Rev. B **102**, 075413 (2020).

[24] S. Venkateswarlu, A. Honecker, and G. Trambly de Laissardière, Phys. Rev. B **102**, 081103(R) (2020).

[25] S. Yuan, H. De Raedt, and M. I. Katsnelson, Phys. Rev. B **82**, 115448 (2010).

[26] G. Yu, Z. Wu, Z. Zhan, M. I. Katsnelson, and S. Yuan, npj Comput. Mater. **5**, 122 (2019).

[27] S. Fang, R. Kuate Defo, S. N. Shirodkar, S. Lieu, G. A. Tritsaris, and E. Kaxiras, Phys. Rev. B **92**, 205108 (2015).

[28] E. Cappelluti, R. Roldán, J. A. Silva-Guillén, P. Ordejón, and F. Guinea, Phys. Rev. B **88**, 075409 (2013).

[29] J. Silva-Guillén, P. San-Jose, and R. Roldán, Appl. Sci. **6**, 284 (2016).

[30] R. Roldán, M. P. López-Sancho, F. Guinea, E. Cappelluti, J. Á. Silva-Guillén, and P. Ordejón, 2D Mater. **1**, 034003 (2014).

[31] S. Huang, X. Ling, L. Liang, J. Kong, H. Terrones, V. Meunier, and M. S. Dresselhaus, Nano Lett. **14**, 5500 (2014).

[32] A. A. Puretzky, L. Liang, X. Li, K. Xiao, B. G. Sumpter, V. Meunier, and D. B. Geohegan, ACS Nano **10**, 2736 (2016).

[33] A. M. van Der Zande *et al.*, Nano Lett. **14**, 3869 (2014).

[34] K. Liu, L. Zhang, T. Cao, C. Jin, D. Qiu, Q. Zhou, A. Zettl, P. Yang, S. G. Louie, and F. Wang, Nat. Commun. **5**, 4966 (2014).

[35] P.-C. Yeh *et al.*, Nano Lett. **16**, 953 (2016).

[36] S. Carr, D. Massatt, S. Fang, P. Cazeaux, M. Luskin, and E. Kaxiras, Phys. Rev. B **95**, 075420 (2017).

[37] Z. Zhan, Y. Zhang, G. Yu, F. Guinea, J. A. Silva-Guillen, and S. Yuan, Phys. Rev. B **102**, 241106(R) (2020).

[38] S. Plimpton, J. Comput. Phys. **117**, 1 (1995).

[39] LAMMPS, http://lammps.sandia.gov.

[40] J.-W. Jiang, Nanotechnology **26**, 315706 (2015).

[41] A. K. Rappé, C. J. Casewit, K. Colwell, W. A. Goddard III, and W. M. Skiff, J. Am. Chem. Soc. **114**, 10024 (1992).

[42] H. Rostami, R. Roldán, E. Cappelluti, R. Asgari, and F. Guinea, Phys. Rev. B **92**, 195402 (2015).

[43] C. R. Dean *et al.*, Nat. Nanotechnol. **5**, 722 (2010).

[44] H. Li *et al.*, arXiv:2007.06113.

[45] Y. Zhang, T.-T. Tang, C. Girit, Z. Hao, M. C. Martin, A. Zettl, M. F. Crommie, Y. R. Shen, and F. Wang, Nature (London) **459**, 820 (2009).

[46] K. F. Mak, C. H. Lui, J. Shan, and T. F. Heinz, Phys. Rev. Lett. **102**, 256405 (2009).

[47] A. Ramasubramaniam, D. Naveh, and E. Towe, Phys. Rev. B **84**, 205325 (2011).

[48] Q. Liu, L. Li, Y. Li, Z. Gao, Z. Chen, and J. Lu, J. Phys. Chem. C **116**, 21556 (2012).

[49] Z. Zhang, J. Li, G. Yang, and G. Ouyang, J. Phys. Chem. C **123**, 19812 (2019).

[50] K. H. Khoo, M. S. Mazzoni, and S. G. Louie, Phys. Rev. B **69**, 201401(R) (2004).